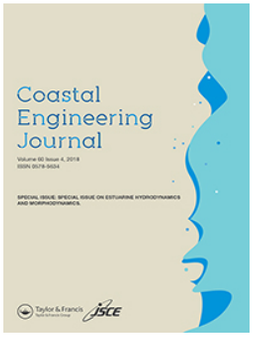

Coastal Engineering Journal

ISSN: 2166-4250 (Print) 1793-6292 (Online) Journal homepage: https://www.tandfonline.com/loi/tcej20

Collapse and recovery process of the sand spit at the Tenryu River mouth on the Pacific Coast of Japan

Yoshimitsu Tajima, Tomohiro Takagawa, Shinji Sato & Satoshi Takewaka

To cite this article: Yoshimitsu Tajima, Tomohiro Takagawa, Shinji Sato & Satoshi Takewaka (2018) Collapse and recovery process of the sand spit at the Tenryu River mouth on the Pacific Coast of Japan, Coastal Engineering Journal, 60:4, 532-547, DOI: 10.1080/21664250.2018.1546264

To link to this article: https://doi.org/10.1080/21664250.2018.1546264

Published online: 04 Dec 2018.

COASTAL ENGINEERING JOURNAL
2018, VOL. 60, NO. 4, 532–547
https://doi.org/10.1080/21664250.2018.1546264

ORIGINAL RESEARCH PAPER

OPEN ACCESS Check for updates

Collapse and recovery process of the sand spit at the Tenryu River mouth on the Pacific Coast of Japan

Yoshimitsu Tajima [a], Tomohiro Takagawa [b], Shinji Sato [a] and Satoshi Takewaka [c]

[a]Department of Civil Engineering, School of Engineering, The University of Tokyo, Tokyo, Japan; [b]Marine Information and Tsunami Department, Port and Airport Research Institute, Yokosuka, Japan; [c]Department of Engineering Mechanics and Energy, Faculty of Engineering, Information and Systems, University of Tsukuba, Tsukuba, Japan

ABSTRACT

This paper investigates the collapse and recovery processes of the sand spit at the Tenryu River mouth on the Pacific Coast of Japan, when two characteristic typhoons, Man-Yi and Fitow, passed over the study site in the year 2007. Although these two typhoons caused equally high storm waves, these two events were different in principal wave directions and in the amount of river discharges. As a result, Man-Yi collapsed the sand spit, while Fitow rather enhanced the recovery of the sand spit. Successive still images recorded by six field cameras were analyzed to investigate the dynamic morphology change of the river mouth for 2 months during which these two events had occurred. Comparisons of obtained topography changes and various hydrodynamic characteristics yielded several findings: (i) the sand spit was breached approximately 6 h after the peak of flow velocity and 2 h after the peak of the water head difference across the sand spit; (ii) the breached part of the sand spit was refilled by wave-induced shoreward sediment transport; and (iii) a core sample showed three clear layers of graded sedimentary structures of gravel, which correspond to the number of observed high waves overtopping the sand spit.

ARTICLE HISTORY
Received 22 December 2017
Accepted 1 November 2018

KEYWORDS
Sand spit; morphology change; storm wave; flood; image-based monitoring

1. Introduction

An estuary plays an important role in the fluvial system and the prediction of overall characteristics of sediment transport, and the resulting morphology change around the river mouth is one of key tasks for better planning and design of sustainable coastal conservation and protection measures. Waves, wave-induced currents, tides, and river flows may interact with each other, and such a complex hydrodynamic field may cause a dynamic morphology change around the river mouth. Morphology changes around the river mouth also have significant influence on the surrounding hydrodynamics and sediment transport characteristics. It should also be noted that severe coastal events, such as tsunami, flood, storm waves and surges, may cause significant and partially irreversible morphology change and may alter the interactive features of the surrounding hydrodynamics, sediment transport, and morphology change characteristics (e.g. Sawamoto and Shuto, 1988, Watanabe and Tanaka, 2003 and Nishihata et al. 2007). Tanaka et al. (2012), for example, investigated the significant topography change induced by the 2011 Great East Japan Earthquake Tsunami and noted that estuaries were highly susceptible to erosion against tsunami, and deformed bathymetry may have significant impacts on the future sediment budget of the surrounding coast.

The collapse and recovery processes of a sand spit at the river mouth are one of the key features of the above-mentioned morphology changes around the river mouth. Dynamic morphology change and nearshore waves, however, make it difficult to install observation devices such as wave gauges for the quantitative monitoring of various phenomena. A laboratory experiment can be one of the options to compensate for such a difficulty of field observation. Coleman, Andrews, and Webby (2002), for example, investigated the breaching process of noncohesive homogeneous embankment due to overtopping flows through a flume experiment. Parkinson and Stretch (2007) conducted a laboratory experiment in a rectangular basin to investigate the breaching process of temporarily opened estuary due to slowly varying outflow. Most of these experiments, however, are based on the assumption of simplified conditions and may not be applicable to investigation of more complex phenomena, such as the interactive features of waves, currents, and changing morphology around the spit. Observation techniques based on video images (e.g. Lippmann and Holman, 1989) have been developed, and many studies have applied such image-based techniques to the monitoring of estuaries (e.g. Morris, Davidson, and Huntley, 2001; Siegle, Huntley, and Davidson, 2007).

CONTACT Yoshimitsu Tajima yoshitaji@coastal.t.u-tokyo.ac.jp

Other studies developed some image-based monitoring system at the Tenryu River mouth located along the Pacific Coast of Japan and, combined with other available data, have investigated various characteristic phenomena at the Tenryu River mouth at different temporal and spatial scales. Focusing on long-term and macro-scale phenomena, for example, Liu, Tajima, and Sato (2008) estimated the time-varying land area of the sand spit before and after the flushing event. Liu, Tajima, and Sato (2010) also investigated the long-term trend of observed shoreline change through the analysis based on empirical orthogonal function. Ahmed, Sato, and Tajima (2014) compared observed shoreline change with the properties of sampled sand grains, such as diameter, material, and thermo-luminescence of each grain, to investigate the characteristics of littoral sediment transport. Focusing on the relatively shorter-term phenomena, Takewaka (2016), on the other hand, analyzed the data recorded by X-band radar and investigated the flushing process of the sand spit during the flood in 2010. Takagawa et al. (2011) also analyzed the X-band radar data to investigate the characteristics of overtopping waves on the sand spit. Tajima, Liu, and Sato (2009) focused on the flushing process of the sand spit and investigated the relationship between time-varying hydrodynamic characteristics and deformation of the sand spit. Tajima et al. (2011) investigated how the tracer sand and gravels move around the deforming sand spit. Nurfaida and Sato (2015) extracted edge wave components through observation of the fluctuating shoreline profiles and investigated the influence of edge waves on the observed morphology change of the sand spit.

Following these earlier studies, this study focuses on both the collapse and recovery processes of the sand spit before and after the two characteristic typhoons, Man-Yi and Fitow, respectively approached the Tenryu River mouth. Figure 1 shows the tracks of Man-Yi and Fitow in the year 2007. As seen in the figure, Man-Yi migrated north-eastward along the southern edge of the main island of Japan and neared the Tenryu River mouth in the daytime of July 15, while Fitow migrated northward and approached the river mouth around the midnight of September 7. While these two typhoons induced equally high storm waves, these two events were different in the following two characteristics: (i) the principal wave direction under Man-Yi was south–southwest (SSW), while the one under Fitow was south–southeast (SSE), and (ii) Man-Yi brought heavy rainfall and caused severe river discharge with a peak of 8700 m^3/s, while Fitow yielded less river discharge. In addition to image-based analysis, this study utilizes various *in situ* data, such as bathymetry, hydrodynamics, and core samples, to

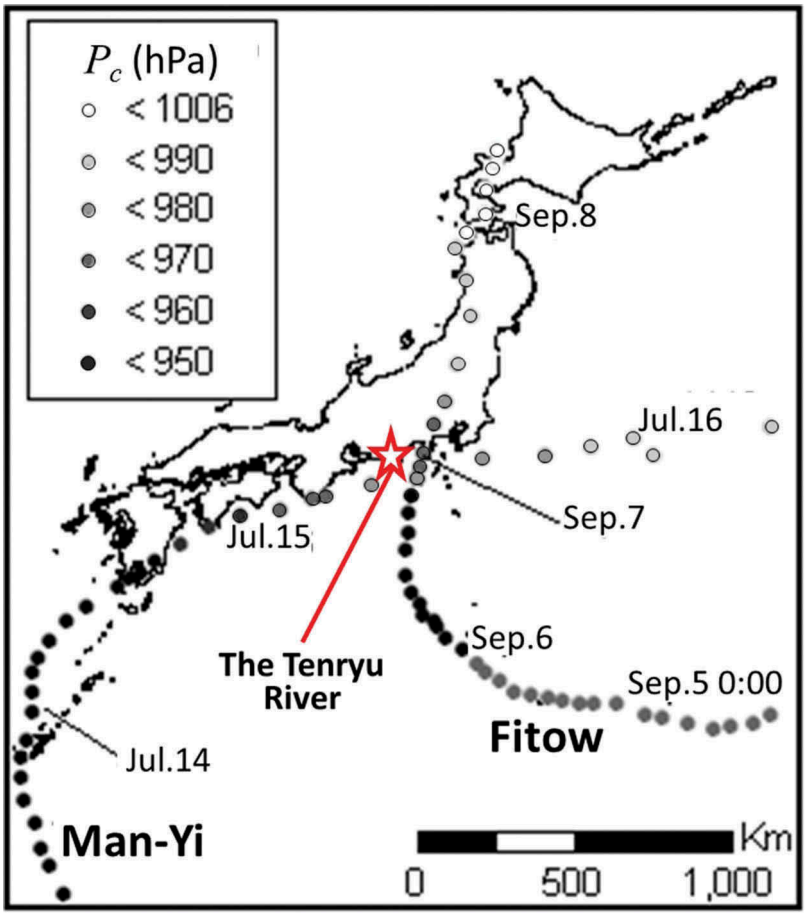

Figure 1. Tracks of two typhoons, Man-Yi and Fitow, and the location of the Tenryu River mouth.

further explore the collapsing and recovery processes under these two contrasting typhoons.

2. Field survey around the Tenryu River mouth

This section outlines the series of intensive field surveys around the Tenryu River from July to September in the year 2007.

2.1. Setups of monitoring and field surveys

Figure 2 shows the setup of the field monitoring. In the figure, black solid circles indicate the locations of six installed field cameras, and arrows with characters from C1 to C6 respectively show the horizontal directions of the installed field cameras. Each of these field cameras recorded successive still images with time intervals of 1.2 s. The circle with the character X indicates the location where the X-band radar was installed (Takewaka 2016). Bed-level profiles across the sand spit were measured along 10 respective lines, shown in thick red lines in the figure with capital letters from A to J. These cross-section profiles were measured along the same lines on several separate days after the attack of Man-Yi. The shoreline profile shown in Figure 2 was recorded by a hand-held GPS on July 19, 4 days after the event, along the line with a bed level of approximately 0 m above the Tokyo Peil (T.P.) +0 m. As seen in the figure, the sand spit was breached around line D. Water depth at this breached part of the sand spit was also measured by GPS sonar on July 23 and August 9 before the area was refilled by sand and gravel. Finally, a thin rectangular core sample was extracted at this breached and refilled part of the sand spit.

2.2. Image analysis

This section outlines the present image analysis for quantitative estimations of shoreline profiles. From successive images with a time interval of 1.2 s, 10-min-averaged images were first developed by averaging the RGB values of each pixel of 500 successive images. Obtained 10-min-averaged images were then rectified based on the horizontal coordinates around the Tenryu River mouth. Rectified images obtained from different field cameras were then combined as a single top-view image based on the identical horizontal coordinates. Figure 3 shows an example of the combined 10-min-averaged images of three different cameras. Images used in Figure 3 were recorded on July 5, 2007, just before the attack of Man-Yi.

For image rectification, this study applied the procedure presented by Tajima, Liu, and Sato (2009) outlined below. The geometric relationship between pixel coordinates of the image, u_i (i = 1,2), and real-world coordinates, x_j (j = 1,2,3), are determined by the following equations (Holland et al., 1997).

$$u_{*i} = \lambda_i(u_i - u_{0i}) = -f_i \frac{m_{ij}(x_j - x_{cj})}{m_{3j}(x_j - x_{cj})} \quad (1)$$

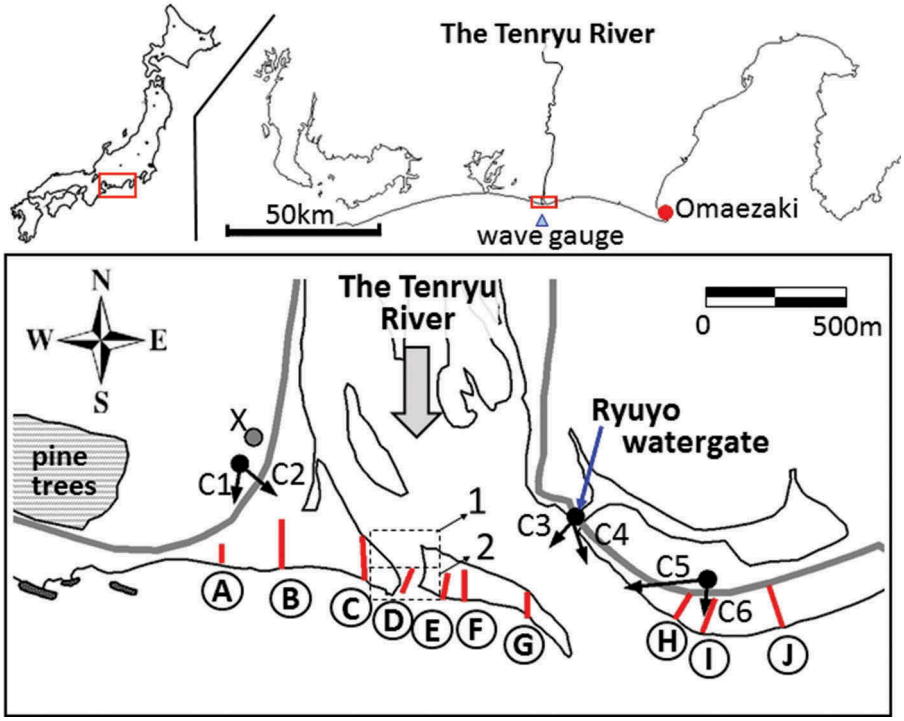

Figure 2. Setups of the field monitoring system around the Tenryu River mouth.

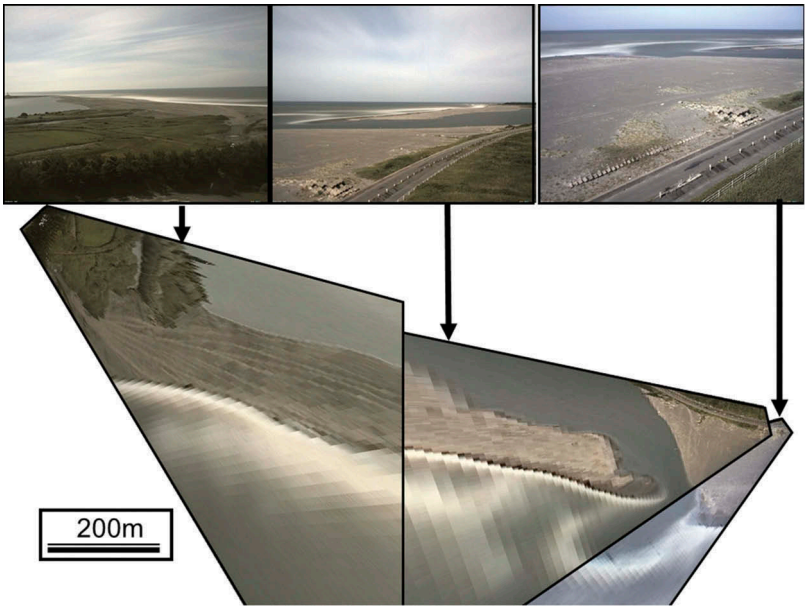

Figure 3. Examples of recorded images and the combined top view image of the river mouth.

Here, f_i is the effective focal length combined with scale factors in horizontal and vertical directions, respectively; u_{0i} is the center-coordinate of the image; m_{ij} is a coefficient determined as functions of camera angles, ϕ_k ($k = 1,2,3$), and the position of the camera, x_{cj}; and λ_i is the coefficient accounting for the image distortion dependent on lens specifications, which should be given or determined separately in advance. All the other parameters, f_i, ϕ_k, and x_{cj} were calibrated based on several reference points where both the field coordinates of the target and corresponding pixel coordinates are known. These optimum parameter values were iteratively estimated based on the following the first-order Taylor series of (1).

$$\Delta u_{*i} = \frac{\partial u_{*i}}{\partial x_{cj}} \Delta x_{cj} + \frac{\partial u_{*i}}{\partial \phi_k} \Delta \phi_k + \frac{\partial u_{*i}}{\partial f_i} \Delta f_i \qquad (2)$$

Here, the left-hand side of (2) is determined as a the difference between known pixel coordinates and estimated pixel coordinates. The least-square method was then applied for estimation of the best combinations of Δx_{cj}, $\Delta \phi_k$ and Δf_i, which determine modification amount of each parameter. Modified parameters were applied again to (1), and the whole procedure was repeated until the estimated errors of image coordinates reached below certain expected criteria. Following Tajima, Liu, and Sato (2009), this study also applied the following weight function so that relative errors of each reference point are scaled not by image coordinates, but by the field coordinates.

$$W_i = \left((\partial u_i / \partial x_1)^2 + (\partial u_i / \partial x_2)^2 + (\partial u_i / \partial x_3)^2 \right)^{-1/2} \qquad (3)$$

3. Observed results and discussions

3.1. Overall topography change characteristics before and after Man-Yi and Fitow

To overview characteristic topography change before and after the attacks of Man-Yi and Fitow, shoreline profiles were quantitatively extracted from obtained images around the river mouth through the following procedures: (i) select images recorded when the tide level was at T.P. +0 m; (ii) rectify selected images based on horizontal *XY*-coordinates at the elevation, T.P.+0 m; (iii) combine rectified images recorded at the same time (Figure 3); and (iv) extract *XY*-coordinates of shoreline profiles from the obtained image. Here, the shoreline location in each image was determined around the land–sea boundary where the cross-shore variation of the pixel brightness reaches its peak. Figure 4 compares shoreline profiles extracted from these images recorded on different days from July to December 2007. Shaded areas shown on both side of the figure indicate the domains where the shoreline location was extracted from the X-band radar image recorded at respective time. The shoreline change analysis discussed in the following section is based on the shoreline extracted from the 10-min-averaged camera images as shown in Figure 3. Although 10-min-averaged images reasonably cancel the error of extracted shoreline location due to instantaneous wave runup, extracted shoreline locations are still affected by spatial variation of the mean water level induced by other hydrodynamic features such as wave setup, tidal current, and river flow. According to the comparison of the water levels at landside and at seaside of the sand spit, as discussed later with Figure 10, the difference of these

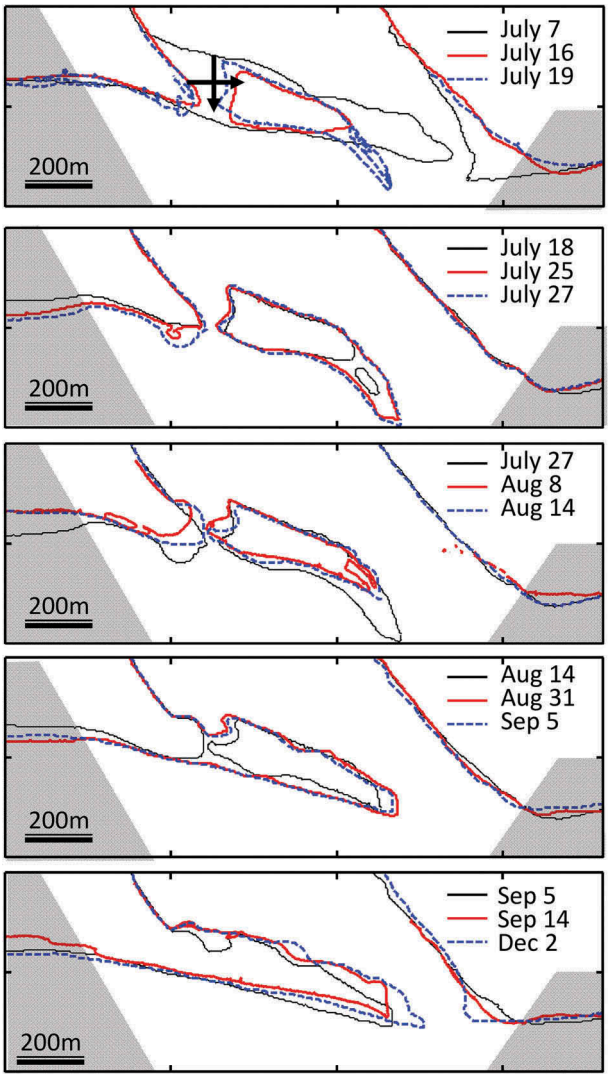

Figure 4. Comparison of extracted shoreline profiles from July 7 to December 2.

water levels, which reflects the influence of aforementioned hydrodynamic features, is at most 30 cm when the tide level is at around T.P. +0 m. Since the observed near shore bed slope is around 1/10, a possible error of the estimated shoreline location due to the influence of such local variation of the mean water level should be within a few or several meters. The left three panels of Figure 5 show the bathymetries around the Tenryu River mouth respectively measured in February, August, and October 2007. The bathymetry data in these figures was obtained by Ministry of Land, Infrastructure, Transport and Tourism of Japan. According to their unpublished report, the water depth was measured by the narrow multi-beam echo sounder (Sea Bat 9001) and the error due to boat motion was corrected based on the data obtained by an inclinometer, a heading sensor, and a motion detector, installed on the same boat. In the shallow water with water depth of less than 50 cm, RTK-GPS was used to directly measure the bed level. It was confirmed through comparison of repeatedly measured data at the same location that the accuracy of the obtained bed level was less than 2 cm in the shallow water and less than 20 cm in the area deeper than 50 cm, respectively. The present study focuses on understanding of the overall erosion and sedimentation characteristics due to this bleaching event and the use of these bathymetry data with aforementioned accuracy should be reasonably acceptable. The right two panels of Figure 5 show the difference in bed levels from February to August and from August to October 2007, respectively. In these panels, the red color indicates the area where the bed level was elevated, i.e. sand was deposited, the blue color indicates the area where the bed level was lowered, i.e. eroded, and the white color indicates the area where the bed level change was less than 50 cm. Contour lines respectively indicate the bed level change of ±50 cm, 100 cm, 200 cm, and so on, with level intervals of 100 cm.

Figure 6 shows the time-varying wave conditions and river discharge. The second panel of Figure 6 is the time-varying river discharge at the Kashima water level station located approximately 25 km upstream from the Tenryu River mouth. The river discharge shown in the figure is based on the measured water level and the stage-discharge rating curve at Kashima station. Since there are no major inflows from Kashima to the river mouth, the flow rate at Kashima should be nearly equivalent to the one around the river mouth, although there should be certain time lags. The bottom three panels of Figure 6 show the time variations of significant wave height, directions, and period, respectively, measured by the wave gauge installed at approximately 5 km offshore from the Tenryu River mouth with water depth of 40 m. In these panels, the wave data measured at Irozaki, located approximately 100 km east of the Tenryu River mouth, were also plotted in thin blue dashed lines to cover the missing data at the offshore of the Tenryu River mouth. For comparison, the top panel of Figure 6 also shows the time variations of the land area in the rectangular domains of 1 and 2 shown in Figure 2. The land area in each rectangular domain was computed based on the shoreline profiles shown in Figure 4, and the top panel of Figure 6 shows the change of the land area based on the one recorded on July 9, just before the attack of Man-Yi.

As seen in Figure 6, no event of significant river discharge was recorded over the study period from July to December 2007, except the one on July 15, when Man-Yi approached the Tenryu River mouth and caused the peak river discharge of approximately 8700 m^3/s. Equally large wave heights were observed around July 15 and September 8 when Man-Yi and Fitow, respectively, hit the site, while the peak wave directions of these two events, SSW under Man-Yi and SSE under Fitow, were different. Relatively high waves

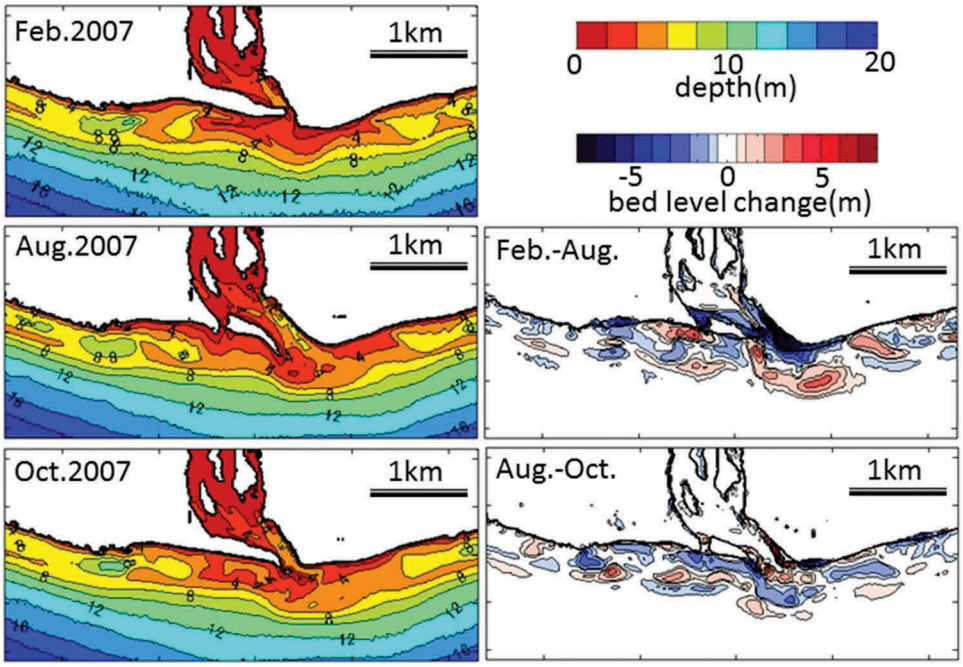

Figure 5. Bathymetries around the Tenryu River mouth measured respectively in February, August and October (left) and the bed level difference from February to August and August to October (right).

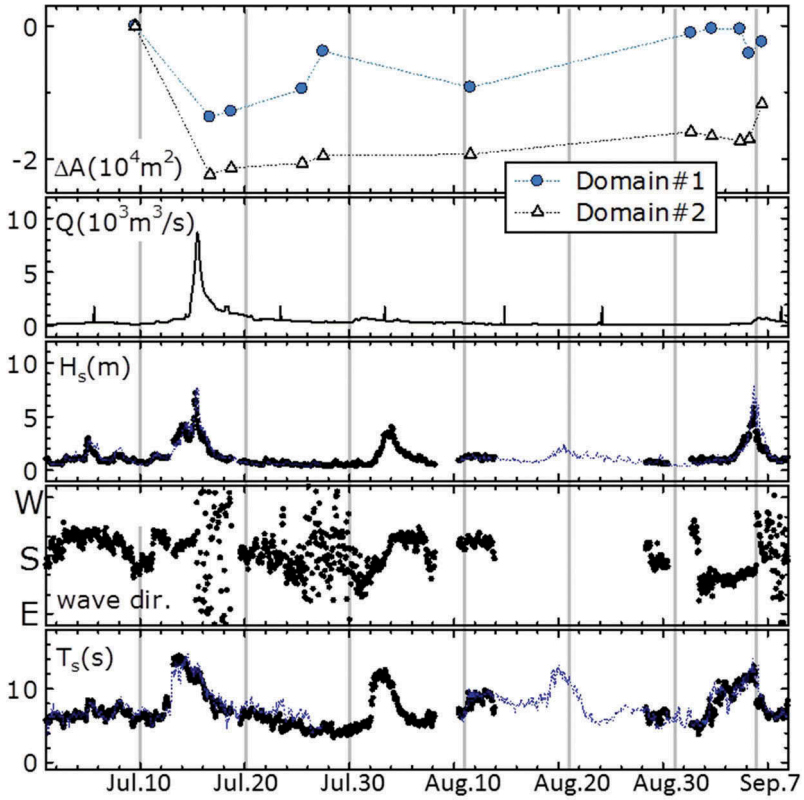

Figure 6. Time series of (1) land area in the rectangular domain #1 and #2 shown in Figure 2; (2) river discharge at Kashima; (3) significant heights, (4) principal directions, and (5) significant period of waves recorded at the offshore wave gauge at the Tenryu River mouth.

were also observed from August 1 to 2, with a significant wave height of approximately 3.5 m and principal direction changing from SSE to SSW.

As seen in Figure 4, the shoreline profile of the sand spit was largely deformed from July 9 to 16, i.e. during the attack of Man-Yi. It is also found that the shoreline on the upper side, i.e. upstream side, of the spit moved seaward, while the shoreline on the seaside of the spit had little movement. It should also be noted that the shoreline on the landside of the spit showed little movement after

July 16 until September 4, i.e. just before the landfall of Fitow. It is also confirmed from the top panel of Figure 6 that a significant decrease of the land area in rectangular domain #2 occurs only from July 7 to 16. These observed features indicate that collapse of the sand spit was dominantly induced by the river discharge.

Comparison of the shoreline profiles on July 16 and 19 shows that the eastern tip of the sand spit quickly developed and extended southeastward within 3 days. It can be deduced from this feature that a large amount of discharged sand was deposited relatively close to the river mouth and was quickly transported back to the shore.

This deduction can also be supported by the comparison of measured bathymetry change from February to August of 2007, shown in Figure 5. For example, significant erosion is observed behind the sand spit and around the river mouth, while significant depositions are observed just seaside of the breached part and eastern tip of the sand spit.

3.2. Collapse process of the sand spit under Man-Yi

Figure 7 shows four combined images of the collapsing sand spit at 17:00 on July 14, 12:00, 14:00, and 17:00 on July 15, respectively, based on the time in Japan, i.e. UTC+9:00 h. Images in Figure 7 were rectified on the same horizontal *XY*-coordinates, but the vertical elevation of the horizontal plane of each image was set to the instantaneous water surface level at the time when each set of images was recorded. Horizontal coordinates of these rectified images are therefore consistent with each other if the elevation of the object in the image is at water surface level in each image. Shorelines are located at the water level in each image, and thus shoreline profiles extracted from each image can be compared with each other. The instantaneous water level of each image was obtained from the gauge installed at the Ryuyo water gate located just inside the river mouth, as shown in Figure 2.

Figure 8 shows the time series of the following hydrodynamic characteristics: (i) the river discharge, i.e. hydrograph, at Kashima observation station; (ii) the water level at Kaketsuka station, η_K, located approximately 3 km upstream from the Tenryu River mouth; (iii) the water levels, η_R and η_O, recorded at the Ryuyo water gate and at offshore wave gauge, respectively; (iv) the difference of water levels at the Ryuyo water gate and offshore wave gauge, i.e. $\Delta\eta$ =

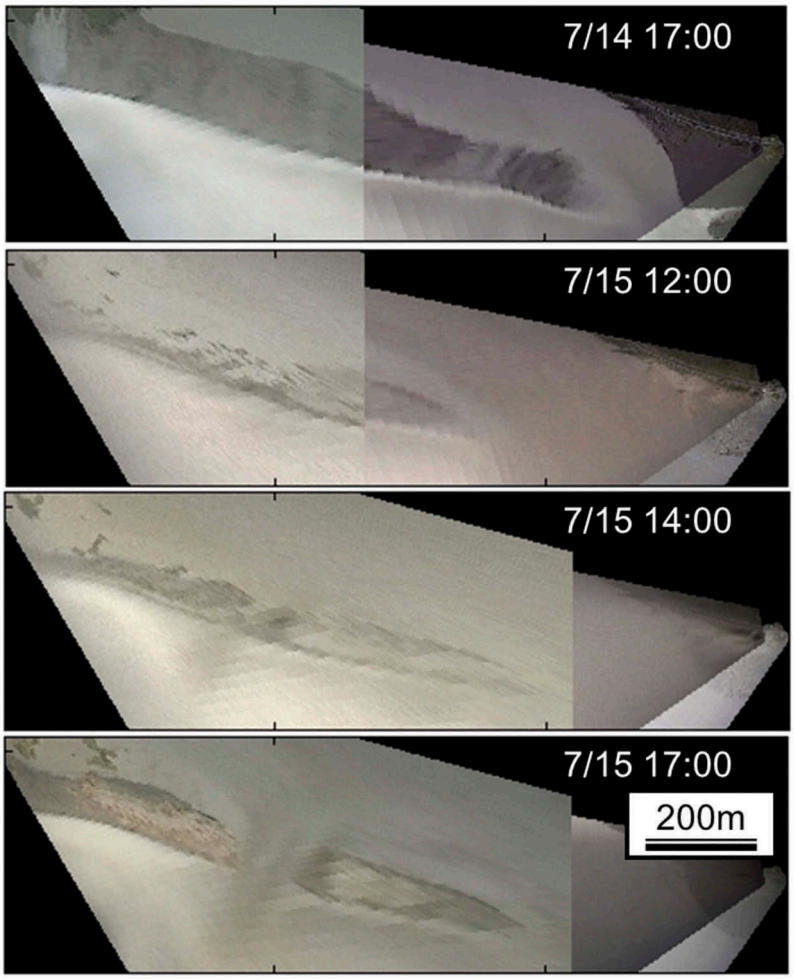

Figure 7. Top view of the sand spit during the flood event under Man-Yi.

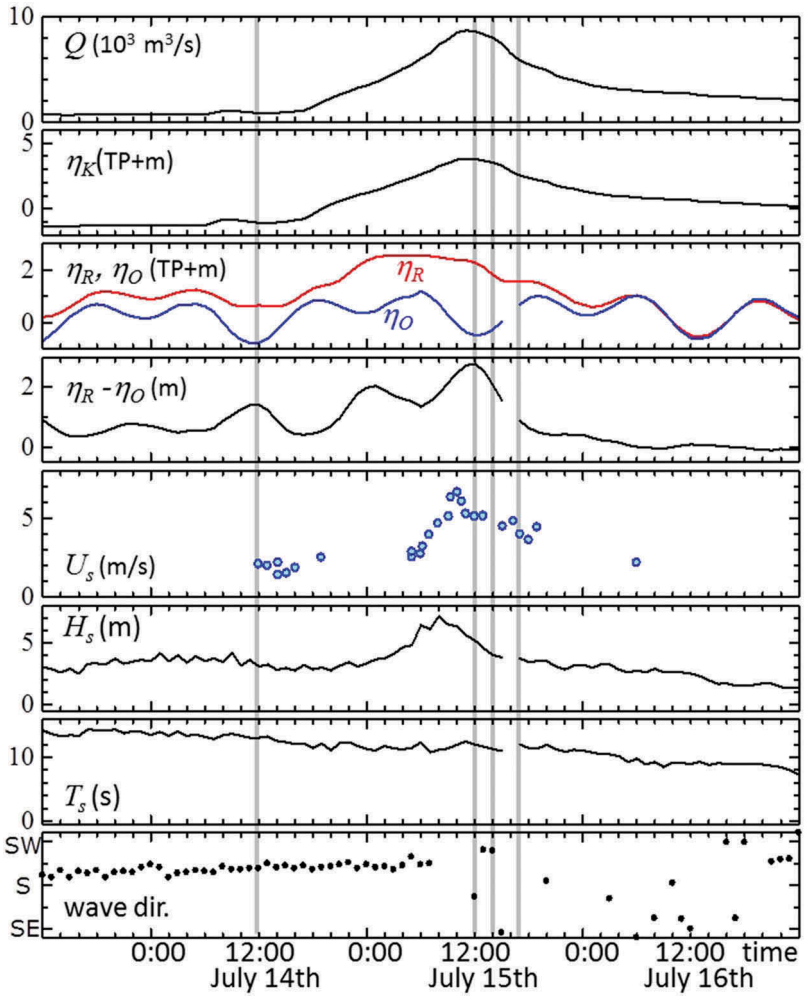

Figure 8. Time series of (1) the river discharge at Kashima; (2) water level at Kaketsuka; (3) water levels at Ryuyo water gate and offshore; (4) difference of water levels at Ryuyo and offshore; (5) surface water velocity; (6) significant height, (7) period and (8) principal directions of waves recorded at the offshore wave gauge of the Tenryu River mouth. Vertical four lines indicate the time at 12:00 on July 14 and 12:00, 14:00, and 17:00 on July 15, respectively. The highest elevation of the sand spit is around TP +4 m.

η_R–η_O; (v) surface flow velocity at the river mouth, U_s; (vi and vii) significant wave height and period, H_s and T_s; and (viii) principal wave directions at the offshore wave gauge. Four vertical thick lines behind Figure 8 respectively indicate the recording times of the four rectified images shown in Figure 7. Surface water velocities, U_s, shown by solid circles in Figure 8, were estimated from the images recorded by camera C4 through conducting the following procedures. Time-varying spatial positions of the floating debris were first traced from successive still images. Extracted pixel coordinates of these debris were then transferred to the horizontal *XY*-coordinates from Equation (1) with the elevation, x_3, specified by the instantaneous water level of the recorded image. The horizontal distance of the identical debris in two successive images yields the horizontal velocity vector components of the floating debris. Finally, these obtained velocities of each debris were averaged over the period of 5 min to yield U_s, shown in Figure 8. Figure 9 shows an example of the image recorded by camera C4 and tracks of floating debris shown as white solid lines and circles on the rectified image. As seen in the figure, tracks of each debris are nearly parallel to each other. Twelve benchmarks were used to calibrate the best-fit rectification parameters in Equation (1), and the rms error of the estimated distances of each two of these benchmarks was approximately 4.6%.

As seen in Figure 8, the water surface level at Kaketsuka, η_K, reached its peak at approximately 12:00 on July 15, 2 h after the peak discharge at Kashima. The time-varying water level at Ryuyo, η_R, on the other hand, is affected by the time-varying tide level and reached its peak at approximately 2:00 on July 15, and this peak water level remained high for 12 h until 12:00, i.e. the peak time of η_K. The water-level difference between the inside and outside of the estuary, $\Delta\eta = \eta_R$–η_O, had the peak at approximately 12:00 while the surface water velocity at the river mouth reached its peak approximately 2 h earlier, i.e. at 10:00. According to the recorded images, the erosion of the eastern tip of the sand spit started approximately 10:00. The river mouth was then significantly widened by 12:00, as shown in

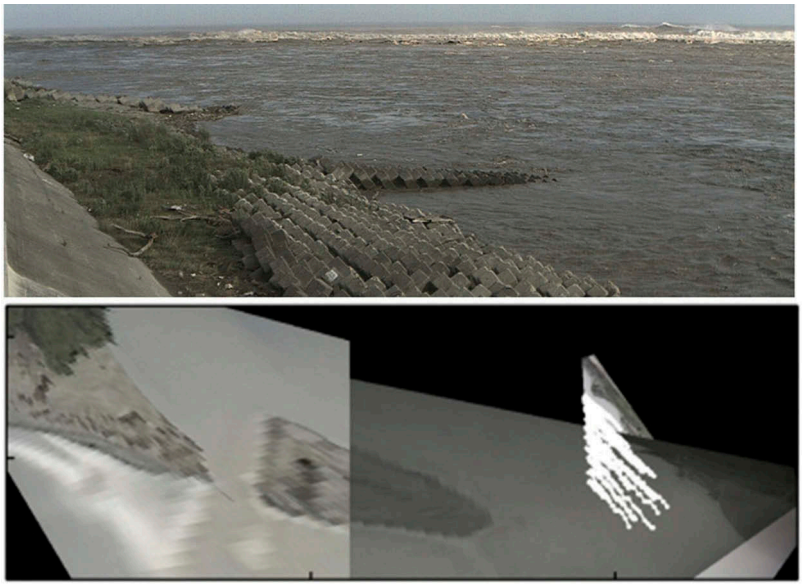

Figure 9. Example of recorded image by the camera, C4 (top), and rectified image with tracks of traced floating debris (bottom).

Figure 7. At 12:00, the west part of the spit was not yet breached, and the darker turbid flow was first observed on the seaside of the breached part of the sand spit at 14:00. At 17:00, the western middle part of the sand spit was fully breached and the upstream side of the shoreline along the sand spit was also eroded. It should be highlighted that the sand spit collapsed at two parts: (i) at the eastern tip and (ii) at the middle-western part with a clear time lag. Table 1 summarizes the observed timings of hydrodynamic and morphological characteristics around the river mouth under the severe discharge event induced by Man-Yi. As summarized in the table, no significant morphology change was observed at the peaks of either η_R or H_s, and the significant erosion of both sides of the river mouth started at 10:00 when U_s reached its peak. On the other hand, the initial indication of the breach of the western part of the sand spit, i.e. the turbid flow, was observed at 14:00, i.e. approximately 4 and 2 h after the peaks of U_s and $\Delta\eta$, respectively. One of important triggers of the sand spit breach may be the water head difference across the spit, which may also enhance the flow velocity over the spit.

As seen in the right middle panel of Figure 5, depositions of discharged sand are observed mainly at two locations: one at the offshore eastern side of the river mouth and the other near the shoreline and slightly west side of the breached part of the sand spit. As shown in Figure 8, the river flow velocity was at its peak at 10:00 on July 15 and the river mouth was largely widened about 2 h later, i.e. at 12:00 as seen in the second panel of Figure 7. Eastward movement of the deposited sand at the offshore of the river mouth, shown in the right middle panel of Figure 5, is also consistent with the dominant SSW wave direction when the peak flow velocity was observed at the river mouth. When the western part of the sand spit was breached, on the other hand, the flow velocity was already decreased as shown in Figure 8. Decreased flow velocity may then deposit the sediment near the shore with a relatively shallower water depth. This sand may be quickly transported back to the shore under relatively milder waves after the event, and then transported westward along the shore by wave-induced nearshore currents. The total amount of deposited sediments around the offshore of the river mouth was about 240,000 m^3. Since this volume accounts for only the deposited sediments, which include the sediment supplied from the eroded sand spit, the sediment supply from the upstream of the Tenryu River should be much less than 240,000 m^3. According to Huang (2011), the sediment discharge under a similar flood event along the Tenryu River before constructions of the Sakuma dam was approximately 8×10^5 m^3/year. This feature may indicate a significant decrease of the sediment supply from the upstream of the Tenryu River in recent years.

Table 1. Summary of observed hydrodynamic and morphological characteristics at different time.

Time	Hydrodynamic characteristics	Morphological characteristics
2:00	Peak of η_R	–
8:00	Peak of H_s	–
10:00	Peak of U_s	Erosion started at the river mouth
12:00	Peak of $\Delta\eta = \eta_R - \eta_O$	The river mouth was widened
14:00	Decrease of η_R	Turbid flow was observed at breaching part of the spit
17:00	Decrease ofU_s	The spit was breached

While the discussions above mainly focused on the impact of changing hydrodynamics on morphology changes, it should also be noted that observed hydrodynamic characteristics are also interactively affected by the changing morphology around the river mouth. On July 15, for example, the peak U_s significantly decreased from 10:00 to 12:00 when the river mouth was widened, and both $\Delta\eta$ and U_s dropped from 14:00 and 17:00 when the western part of the sand spit was breached. Such an influence of the river mouth morphology can also be seen in the tidal characteristics inside the estuary. The top panel of Figure 10 shows a time series of tides at the Ryuyo water gate, η_R, and Omaezaki tidal station, η_{OM}, located approximately 40 km east from the Tenryu River mouth along the Enshu-nada coast. It was confirmed that phases and peaks of the tide recorded at Omaezaki station were nearly equivalent to those measured at the wave gauge offshore of the Tenryu River mouth before the event induced by Man-Yi. The data at Omaezaki was used in this figure simply because a part of the data at the offshore wave gauge was missing after Man-Yi. The middle panel of Figure 10 shows the instantaneous difference of these tide levels, $\eta_{R\text{-}OM}$ as a function of η_{OM}. Blank and solid circles in the figure distinguish the data before and after the bleaching event. As seen in the figure, the water-level difference becomes smaller after the bleaching, i.e. after July 16 and the water-level difference is at most 30 cm after the bleaching when the tide level at Omaezaki is around T.P. +0m. To exclude the influence of the phase lag of observed tidal water levels at these two gauges, the bottom panel of Figure 10 compares peak water levels during both high and low tides at Ryuyo, $\eta_{p,R}$, and Omaezaki, $\eta_{p,OM,}$ before and after the event. Harmonic analysis was respectively applied for estimations of peak tide levels. Before the storm, the difference in peak water levels at Ryuyo and Omaezaki was as high as 25 cm during the low tide. After the storm, on the other hand, the tidal profiles at Ryuyo and Omaezaki are nearly equivalent to each other. The lower water-level difference after the bleaching reduces the seaward flow velocity around the river mouth, and the wave-induced landward sediment transport dominantly causes the redevelopment of the sand spit. This feature indicates that the monitoring of tidal water-level change both at inside and outside of the sand spit can be a good indicator for evaluation of the development of the sand spit.

3.3. Recovery process of the sand spit after Man-Yi

This section focuses on the recovery process of the sand spit after Man-Yi and before the attack of Fitow.

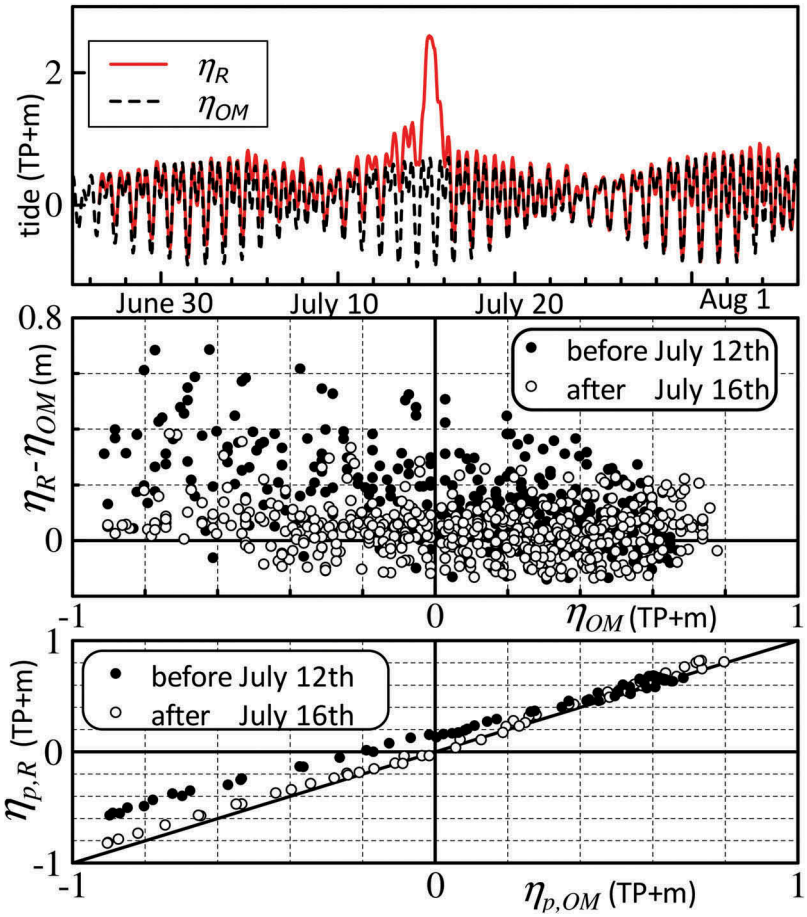

Figure 10. Comparison of tide level and peak tide levels recorded respectively at Ryuyo water gate and at Omaezaki (top: time series, middle: instantaneous tide level at every 10 min, and bottom: peak tide levels).

After the event of Man-Yi, as seen in Figure 6, the observed significant wave height was as high as 1 m until the end of July. Under these relatively mild waves, the eastern tip of the sand spit was extended in the southeastward direction and the land area in rectangular domain #1, A_1, shown in Figure 2, was quickly increased. From August 1 to 3, relatively larger waves with significant wave height of approximately 3.5 m were observed and the land area, A_1, was decreased due to the retreat of the entire shoreline on the seaside of the sand spit. From August 3 to the beginning of September, observed significant wave heights were from 1 to 2 m and A_1 was gradually increased. In contrast to the change of A_1, the land area in rectangular domain #2, A_2, had less time fluctuations and showed a gentle and simple increasing trend. Since domain #2 is not exposed to the nearshore waves, this feature may indicate that wave-associated onshore sediment transport dominantly contributed to the refill of the breached part of the spit. It should also be noted that the land side of the breached part of the sand spit was not filled until the attack of Fitow on September 7.

Figure 11 shows measured cross-shore profiles of the bed level along lines A to J shown in Figure 2. The bed levels were measured four times after the attack of Man-Yi along each cross section, except D, along the breached part of the spit, which was under water until the end of August and was measured only once on November 30. The horizontal axis of these figures indicates a cross-shore distance in the southward, i.e. seaward, directions with the origin set at the shoreline location on July 22, the first day of this bed level survey. Figure 12 also shows cross-shore and alongshore bed levels measured by GSP-sonar at the breached part of the sand spit, indicated by black arrows in Figure 4. The vertical axis of these figures is elevation based on T.P., and as seen in Figure 12, the lowest bed level at the breached part of the sand spit was approximately T.P.-2.5 m.

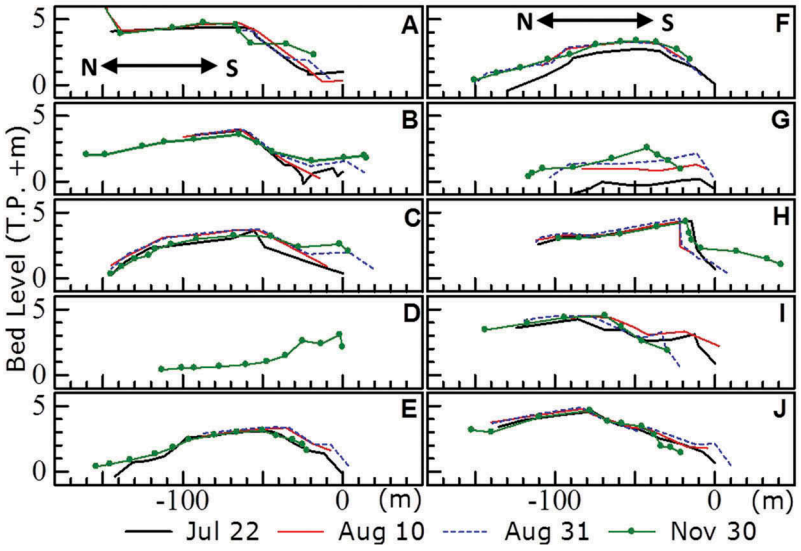

Figure 11. Comparison of measured cross-section profiles along lines A to J shown in Figure 2.

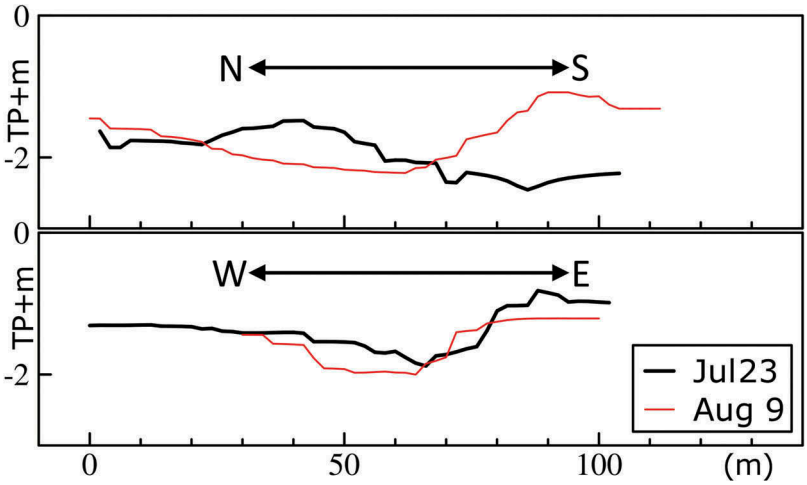

Figure 12. Measured bed level along the arrows shown in Figure 4 at the breached part of the spit: cross-shore direction (top) and alongshore direction (bottom).

As seen in Figure 11, clear deposition is observed around the foreshore of lines B, C, and E, i.e. in the vicinity of the breached part of the sand spit from August 10 to 31. The comparison of cross-shore profiles of the bed levels at the breached part of the spit, as shown in the upper panel of Figure 12, deposition is dominant on the southern side, i.e. the seaside of the cross section from July 23 and August 9. In the alongshore direction, as seen in the lower panel of Figure 12, shown that the deeper portion of the breached opening was shifted westward by approximately 10 m, and this feature indicates the westward alongshore sediment transport. Along lines F and G, the bed levels on July 22 were relatively low compared to those of B, C, and E. The entire bed level along lines F and G was elevated after July 22, while the shoreline locations showed relatively less change. This feature, i.e. relatively stabilized shoreline after the end of July, can also be seen in Figure 4. Based on these observations, one can deduce the following characteristics of the sediment transport: (i) wave-induced landward sediment transport and westward littoral sediment transport were dominant under relatively milder waves after Man-Yi, (ii) wave-induced sediment transport dominantly enhanced the deposition on the entire cross section of the relatively lower sand spit and the foreshore of the relatively higher sand spit, and (iii) the westward littoral sediment transport filled the eastern side of the breached sand spit and caused sedimentation along the coast on the west side of the breach.

3.4. Recovery process of the sand spit under Fitow

Finally, this section discusses the characteristic morphology change under the storm waves induced by Fitow. As previously discussed, the primary difference between Man-Yi and Fitow was that Fitow had less river discharge and the principal directions of storm waves induced by Fitow was SSE whereas the one by Man-Yi was SSW. As a result, observed morphology changes around the river mouth were also significantly different between these two events. For example, comparison of shoreline profiles on September 5 and 14, i.e. before and after the attack of Fitow shows sediment accumulation along the east bank near the river mouth, accumulation near the shoreline on the upstream side of the sand spit, and retreat of the shoreline on the seaside of the sand spit. The entire cross section along line G, shown in Figure 11, was elevated and shifted northward. Figure 13 shows the time variations of the land area change in the rectangular domains 1 and 2 shown in Figure 2 and the wave characteristics recorded at the offshore wave gauge of the Tenryu River. Figure 13 is based on the same data shown in Figure 6 but focuses on the event due to Fitow and the area change shown in the top panel is now based on the area recorded on September 2. As seen in Figure 13, the land area in domain #1, A_1, was first decreased from September 5 to 6 and then increased from 6 to 7. In contrast to this relatively minor area change of A_1, the land area in domain #2, A_2, located on the upstream side of the spit, significantly increased from 6 to 7 although A_2 showed no significant area change before the attack of Fitow. Figure 14 compares rectified images of the sand spit recorded at 9:00 on 5, 6:00 on 6 and 11:00 on September 7, respectively. Tide levels of each image are the same, T.P.+0 m, at the Ryuyo water

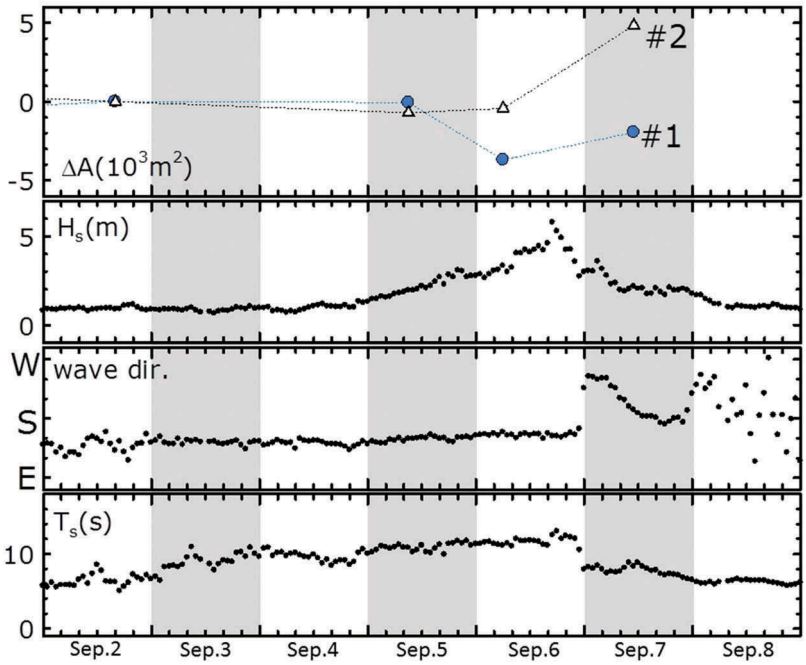

Figure 13. Time-series of the area change in the rectangular domains #1 and #2 shown in Figure 2 and wave properties recorded at the offshore wave gauge of the river mouth.

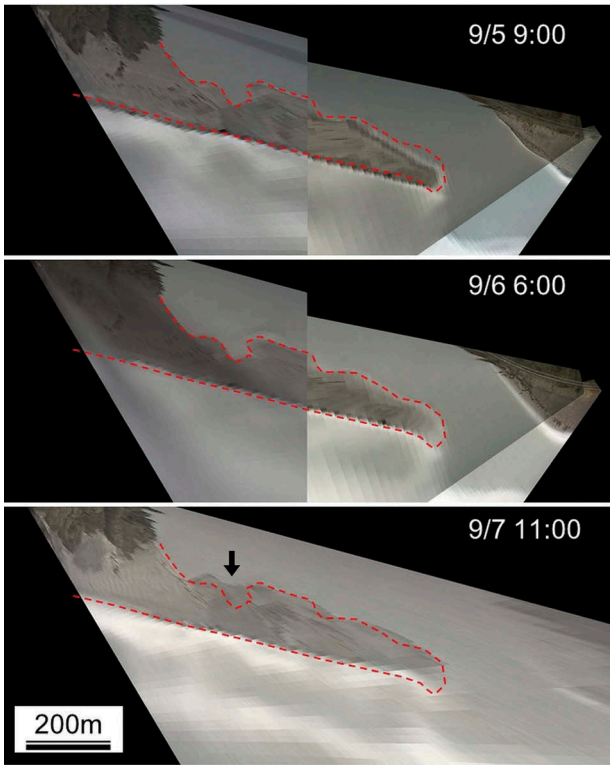

Figure 14. Comparisons of rectified top-view images during the attack of Fitow. Red dashed lines indicate the shoreline profile at 6:00 on September 6 (middle panel), and the arrow in the bottom panel indicates the location where clear sand deposition was observed from the 6th to the 7th.

gate and, for comparison, red dashed lines in the figure indicate the observed shoreline profile of the middle image captured at 6:00 on September 6. As seen in the figure, a part of the upstream side of the spit, indicated by an arrow, was clearly filled from the 6th to the 7th and the entire shoreline on the seaside of the spit slightly retreated from the 5th to the 6th. Severe waves with a SSE principal direction may have induced the westward littoral sediment transport and caused the observed shoreline retreat around the eastern tip of the spit. The shoreline retreat on the western part of the spit and the initial decrease of A_1, on the other hand, may be due to cross-shore seaward sediment transport under relatively high waves. This hypothesis can be supported by the similar shoreline retreat and decrease of A_1, as seen in Figures 4 and 6, in the beginning of August when relatively severe waves with a significant height of approximately 3.5 m were incident on the coast.

In the afternoon of the 6th, the wave height was increased more and these waves started to overtop the lower part of the sand spit. Figure 15 shows the image captured by field camera C2 at 15:00 on the 6th. In the figure, overtopping waves are observed not only at the eastern tip but also at the breached part of the sand spit. It is also seen in the bottom panel of Figure 4 that, from September 5 to 14, the land area was extended on the upstream side of the spit, both around the breached part and the eastern end of the spit where overtopping waves were observed. Based on these observations, it can be deduced that wave-induced landward sediment transport has a dominant influence on the recovery and redevelopment process of the collapsed sand spit and the upstream side of the sand spit was mainly refilled by overtopping waves.

Evidence of such a dominant effect of landward sediment transport induced by overtopping waves was also found in the layers of deposited sediments at the breached part of the sand spit. Figure 16 shows the picture and a sketch of the core sample extracted from the layers of newly deposited sediments at the intersection of the two arrows shown in Figure 4, i.e. at the center of the breached and refilled part of the spit. The core sample was extracted on November 2. The figure also shows the vertical distributions of grain diameters with different cumulative mass fractions, D_5, D_{25}, D_{50}, D_{75}, and D_{95}. Here, grading analysis was performed in each observed layer of the extracted core sample with thickness varying from 5 to 30 cm. As seen in the sketch of the core in Figure 16, there are three characteristic layers, indicated by A, B, and C, and each layer has the following three characteristic structures from the bottom to the top: (i) erosion surface at the bottom of the layer indicated as a thick solid line, (ii) upward coarsening sedimentation layer on top of the erosion surface, and (iii) upward fining sedimentation layer on top of the upward coarsening sedimentation layer. This structure may be developed through (i) erosion under severe waves, (ii) landward transportation and deposition of coarse gravel under severe waves, and (iii) transportation and sedimentation of fine sands under daily

Figure 15. Overtopping waves observed in the image of the camera, C2, recorded at 15:00 on September 6th.

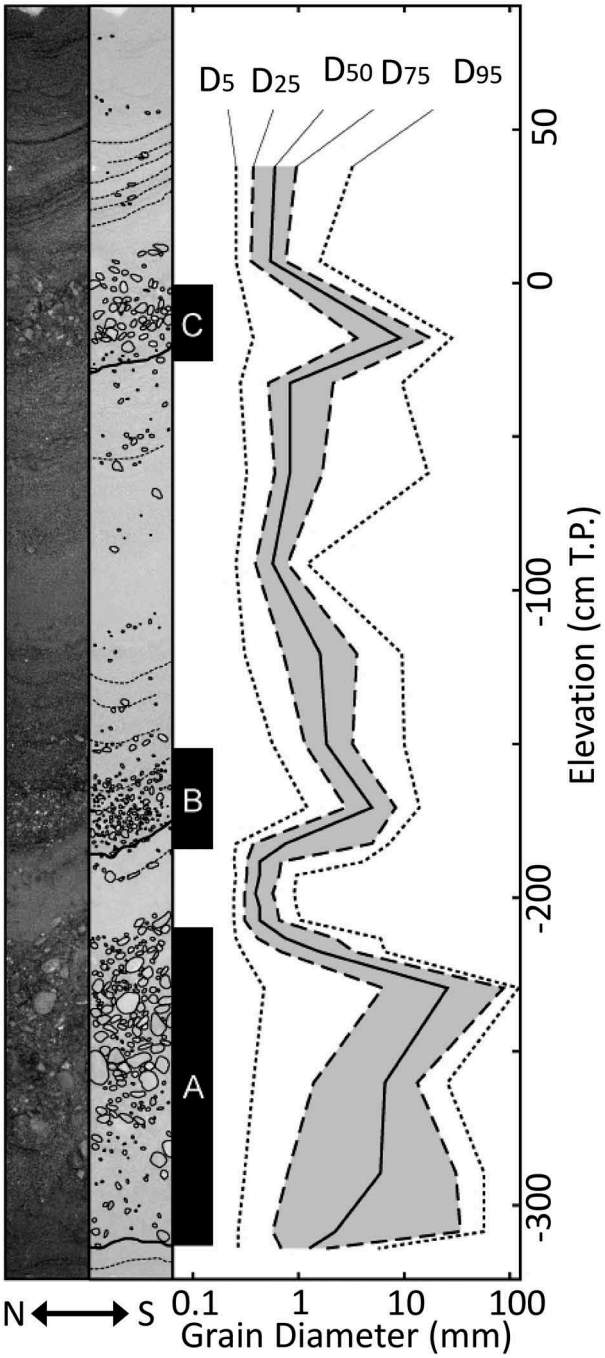

Figure 16. The picture (left) and the sketch (middle) of the extracted core sample and vertical distributions of estimated grain diameters of different cumulative mass fractions. Horizontal axis of the left two panels indicate cross-shore north–south direction.

milder waves. It should also be highlighted that the observed number of layers, A, B, and C, is consistent with the number of events with relatively high waves on August 4, 19 and September 7, during which the breached part of the spit was refilled as indicated in Figure 6. It is also interesting to note that the maximum grain sizes of each layer, A, B, and C, are correlated with the peak significant wave heights of corresponding event, i.e. the storm wave induced by Man-Yi, high waves on August 1 and the storm wave induced by Fitow, respectively.

The core sample also shows laminae sloping in the down northward direction, which indicate that grains were transported northward to develop the sedimentary layer (Allen, 1982). Figure 17 shows a picture taken on the refilled sand spit on August 23 looking in the eastward direction. The bed surface in this picture shows an imbricate structure, i.e. a sedimentary structure in which pebbles are inclined in the same direction. As seen in the picture, pebbles are inclined in the southward, i.e. the seaward direction and, according to Allen (1982), this feature also indicates that the surface bed materials were affected by a northward, i.e. the landward current due to overtopping waves. All these observations indicate that overtopping waves was one of dominant factors to enhance the recovery of the collapsed sand spit at the Tenryu River mouth.

4. Conclusions

This study investigated the collapse and recovery processes of the sand spit at the Tenryu River mouth when typhoons Man-Yi and Fitow approached the river mouth in July and September 2007, respectively. While these two typhoons caused equally high storm waves, they were different in the principal directions of induced waves and the amounts of river discharge. As a result, the storm induced by Man-Yi caused a significant collapse of the sand spit, while Fitow rather enhanced the recovery of the sand spit.

Six field cameras were installed to capture the dynamic morphology changes around the Tenryu River mouth. Recorded successive still images with a time interval of 1.2 s were rectified based on the *XY*-coordinate system on the horizontal plane at the water level, T.P. +0 m. Time-varying shoreline profiles were then extracted from these rectified images. During the flood induced by Man-Yi, floating debris, captured by the field cameras, was traced to obtain the time-varying surface flow velocity at the river mouth. The obtained velocity was then compared with the recorded time-varying water levels inside and outside of the river mouth and with profiles of

Figure 17. A picture taken on the breached and refilled part of the sand spit. The picture was taken on August 23 looking eastward direction.

the sand spit. It was found through comparisons of these data that there was a 4-h time lag between the two characteristic deformation processes of the sand spit: (i) erosion of the eastern tip of the spit and (ii) breach of the western part of the spit. The erosion of the eastern tip of the spit started when the observed surface water velocity reached its peak, while the breach of the sand spit was initiated 2 h after the water head difference between the inside and outside of the estuary reached its peak. It was also found that the observed morphology changes of the river mouth have a significant impact on the surrounding hydrodynamic characteristics, such as flow velocities, tidal responses, and water levels.

Recovery processes of the sand spit after Man-Yi were also investigated through comparisons of time-varying profiles of the sand spit and other data, such as measured cross sections of the spit, bathymetry around the river mouth, core sample of the refilled sediment at the breached part of the sand spit, waves, tides, and river flows. It was found that the collapsed sand spit was refilled by the wave-induced landward sediment transport. The shoreline on the upstream side of the spit was not filled until overtopping waves were observed on the sand spit when typhoon Fitow approached the site. The core sample of refilled sediment extracted at the breached part of the sand spit also showed the evidence of the northward sediment transport under severe waves propagating or overtopping the breached part of the sand spit.

The bleaching and recovery process of the sand spit of the Tenryu River mouth was reasonably captured by the present monitoring system based on multiple time-lapse camera images combined with the other *in situ* data set such as time-series of the water level at landside and seaside of the sand spit, offshore wave conditions, core samples, and a nearshore bathymetry. It was found through this study that the bleaching process was dominantly determined by the river discharge characteristics such as the flow velocity around the sand spit and the water head difference crossing over the sand spit. The recovery process, on the other hand, was dominantly determined by wave-induced sediment transport and it was found that overtopping waves played an important role in expansion of the sand spit. The obtained quantitative data set of the time-varying deformation process of the sand spit and the corresponding hydrodynamic characteristics around should be essential for understanding of the physical mechanism of such phenomena. Some of these observed features may be specific to the case of the Tenryu River mouth and further observations and investigations are needed for better understandings of the overall characteristics of the sand spit deformation. The present remote sensing-based monitoring system can be one of preferred observation techniques because of its applicability for observation of such bleaching and recovery process of the sand spit in other estuaries which have different hydrodynamic and geological characteristics.

Acknowledgment

The authors gratefully acknowledge that a part of this study was supported by The River Foundation, Japan.

Disclosure statement

No potential conflict of interest was reported by the authors.

ORCID

Yoshimitsu Tajima http://orcid.org/0000-0002-1856-4723
Tomohiro Takagawa http://orcid.org/0000-0002-2783-5951
Shinji Sato http://orcid.org/0000-0002-3718-1859
Satoshi Takewaka http://orcid.org/0000-0002-0175-4643

References

Ahmed, M. T. T., S. Sato, and Y. Tajima. 2014. "Quantitative Estimation of Longshore Sediment Transport Based on Thermoluminescence: Two Case Studies around Tenryu and Nile River Mouths." *Journal of Coastal Research* 30 (3): 537–547. doi:10.2112/JCOASTRES-D-13-00050.1.

Allen, J. R. L. 1982. *Sedimentary Structures: Their Character and Physical Basis*, 593. Vol. I. Oxford: Elsevier Scientific.

Coleman, S. E., D. P. Andrews, and M. G. Webby. 2002. "Overtopping Breaching of Non-Cohesive Homogeneous Embankments." *Journal of Hydraulic Engineering* 128 (9): 829–838. doi:10.1061/(ASCE)0733-9429(2002)128:9(829).

Holland, K. T., R. A. Holman, T. C. Lippmann, and J. Stanley. 1997. "Practical Use of Video Imagery in Nearshore Oceanographic Field Studies." *IEEE Journal of Oceanic Engineering* 22 (1): 81–92. doi:10.1109/48.557542.

Huang, G. 2011. "Time Lag between Reduction of Sediment Supply and Coastal Erosion." *International Journal of Sediment Research* 26 (1): 27–35. doi:10.1016/S1001-6279(11)60073-5.

Lippmann, T. C., and R. A. Holman. 1989. "Quantification of Sand Bar Morphology: A Video Technique Based on Wave Dissipation." *Journal of Geophysical Research* 94 (C1): 995–1011. doi:10.1029/JC094iC01p00995.

Liu, H., Y. Tajima, and S. Sato. 2008. "Field Study on the Nearshore Sediment Process around the Tenryu Estuary Using Image Analysis." *Proceedings of the 31st International Conference on Coastal Engineering* 3: 2064–2076. doi:10.1142/9789814277426_0170.

Liu, H., Y. Tajima, and S. Sato. 2010. "Long-Term Monitoring on the Sand Spit Morphodynamics at the Tenryu River Mouth." *Proceedings of the 32nd International Conference on Coastal Engineering*. doi:10.9753/icce.v32.sediment.87.

Morris, B. D., M. A. Davidson, and D. A. Huntley. 2001. "Measurements of the Response of a Coastal Inlet Using Video Monitoring Techniques." *Marine Geology* 175: 251–272. doi:10.1016/S0025-3227(01)00144-X.

Nishihata, T., Y. Tajima, Y. Moriya, and T. Sekimoto. 2007. "Topography Change due to the Dec 2004 Indian Ocean Tsunami - Field and Numerical Study at Kirinda Port, Sri

Lanka." *Proceedings of the 30th International Conference on Coastal Engineering*, 1456–1468.

Nurfaida, W., and S. Sato. 2015. "A Study on Hydrodynamic Characteristics and Resulting Morphological Formation of Sand Spit around the Tenryu River Mouth Based on Image Analysis." *Procedia Engineering* 116: 141–148. doi:10.1016/j.proeng.2015.08.275.

Parkinson, M., and D. Stretch. 2007. "Breaching Timescales and Peak Outflows for Perched, Temporary Open Estuaries." *Coastal Engineering Journal* 46 (3): 267–290. doi:10.1142/S0578563407001605.

Sawamoto, M., and N. Shuto. 1988. "Topography Change Due to Flood and Recovery Process at the Abukuma River Mouth." *Coastal Engineering Japan* 30 (2): 99–117. doi:10.1080/05785634.1988.11924478.

Siegle, E., D. A. Huntley, and M. A. Davidson. 2007. "Coupling Video Imaging and Numerical Modeling for the Study of Inlet Morphodynamics." *Marine Geology* 236: 143–163. doi:10.1016/j.margeo.2006.10.022.

Tajima, Y., H. Liu, and S. Sato. 2009. Dynamic Changes of Waves and Currents over the Collapsing Sandbar of the Tenryu River Mouth Observed during Typhoon T0704, Proc. Coastal Dynamics 2009, Toyo, CD-ROM published by World Scientific.

Tajima, Y., H. Liu, T. Takagawa, and S. Sato. 2011. "Selective Movements of Sand and Gravels and Resulting Dynamic Morphology Changes Observed around the Tenryu River Mouth." *Proceedings of the Coastal Sediments* 2011: 1135–1148. doi:10.1142/9789814355537_0086.

Takagawa, T., Y. Tajima, H. Liu, S. Takewaka, and S. Sato. 2011. "Dynamic Topography Changes of Sand Spit of the Tenryu River Mouth Due to Overtopping Waves." *Proceedings of the Coastal Sediments* 2011:. 1217–1228. doi:10.1142/9789814355537_0092.

Takewaka, S. 2016. "Observation of Whole Flushing Process of a River Sand Bar by a Flood Using X-Bad Radar." *Journal of Marine Science and Engineering* 4 (32). doi:10.3390/jmse4020032.

Tanaka, H., N. X. Tinh, M. Umeda, R. Hirao, E. Pradjoko, A. Mano, and K. Udo. 2012. "Coastal and Estuarine Morphology Changes Induced by the 2011 Great East Japan Earthquake Tsunami." *Coastal Engineering Journal* 54 (1). doi:10.1142/S0578563412500106.

Watanabe, K., and H. Tanaka. 2003. "Recovery Process of Sand Spit at the Natori River Mouth." *Proceedings of International Conference on Asian and Pacific Coasts 2003*. CD-ROM. doi:10.1142/9789812703040_0054.